Reaction Diffusion Manifolds - REDIM

F. C. Minuzzi

1 Model reduction

Model reduction methods are a collection of techniques that use thermodynamic information of the problem to produce a less difficult system to be solved. Almost all strategies will reduce the number of species mass fractions equations to be solved, using ideas that allow that some thermo-kinetics properties can be calculated in function of other ones. One such strategy is the slow manifold approach, which uses the separation of time scale to find an attractive manifold in the state space that describes the system's dynamics.

2 Time scale analysis

Development of skeletal mechanisms may provide a significant reduction in the number of species that are necessary for modelling combustion but, for incorporation in 2D or 3D CFD codes, the number of variables may still be prohibitive [34]. Complex fuels, such as long chain hydrocarbons or alcohols, can contain a significant quantity of isomers[1], which lead to several intermediary species and reactions. A possible overcome to this issue is the time scale analysis.

The kinetic system of ordinary differential equations defines the relation between the production rate of a species and the reaction rates [34]. For an isothermal, spatially homogeneous dynamical system, the concentration change over time can be obtained solving the following initial value problem [31]:

$$\frac{d\mathbf{c}}{dt} = \mathbf{f}(\mathbf{c}, \mathbf{k}), \quad \text{with} \quad \mathbf{c}(0) = \mathbf{c}_0, \tag{1}$$

where $\mathbf{c}(t)$ is the concentration vector, t the time and $\mathbf{k}$ the vector for kinetic parameters, such as Arrhenius coefficient, thermodynamic data, pressure, temperature, etc. The most commom variable used as parameter $\mathbf{k}$ is the reaction velocity coefficient [18, 32, 34]. The right hand side of Eq. (1) can be obtained, for each species i, using

$$f_i(\mathbf{c}, \mathbf{k}) \quad = \quad \sum_{j=1}^{n_r} \nu_{ij} \dot{\omega}_j, \tag{2}$$

where ν_{ij} is the stoichiometric coefficient of species i in reaction j and $\dot{\omega}_j$ is given by

$$\dot{\omega} \quad = \quad k_f \prod_{i=1}^{n_{sp}} [X_i]^{\nu_i'} - k_b \prod_{i=1}^{n_{sp}} [X_i]^{\nu_i''} \tag{3}$$

[1] Species that have the same molecular form, but differs in the structure.

where k_f is the forward reaction rate coefficient and k_b the backwards reaction rate coefficient. Usually, k_b is calculated through the equilibrium constant K_c since, when $\dot{\omega} = 0$, it holds that

$$\frac{k_f}{k_b} = \frac{\prod_{i=1}^{n_{sp}} [X_i]^{\nu_i''}}{\prod_{i=1}^{n_{sp}} [X_i]^{\nu_i'}} = K_c. \tag{4}$$

The chemical equilibrium can be determined by species concentrations or using the variation of the Gibb's function ΔG_T^o

$$K_c = \exp\left(-\frac{\Delta G_T^o}{RT}\right) \tag{5}$$

When the intention is to analyse the consumption/production of a chemical species in a kinetic mechanism of n_r elementary reactions, it is necessary to incorporate the molar rate to the contribution of each one of those. Thus, the relation (3) turns to

$$\dot{\omega}_i = W_i \sum_{j=1}^{n_r} \nu_{kj} \left[k_{fj} \prod_{i=1}^{n_{sp}} [X_i]^{\nu_{ij}'} - k_{bj} \prod_{i=1}^{n_{sp}} [X_i]^{\nu_{ij}''} \right], \tag{6}$$

where the net stoichiometric coefficient $\nu_{kj} = \nu_{kj}'' - \nu_{kj}'$ is calculated in each reaction j.

The molar rate of each species possess the contribution of several reactions that happens extremely fast, leading to highly non-linear and stiff system of equations [24]. The integration of this system in the context of combustion modelling is in many conditions considered prohibitive. Therefore, there is the requirement to simplify the detailed kinetic mechanism without losing the chemical knowledge of important species.

Models for chemical kinetics have several different time scales, which are related to the dynamical behaviour of the model, considering perturbation in the system. Depending on the species, consumption rate can change in different orders of magnitude within a mechanism, and one example is the intermediate radicals, which react faster than stable species. This difference enhances the stiffness of the calculations and leads to numerical problems when solving the system of ODE (1). The separation of time scales is an interesting approach to overcome this problem, since then fast variables can be determined by the slow variables values.

For a general kinetic mechanism, the lifetime τ of a species i is given by

$$\tau_i = -\frac{1}{J_{ii}}, \tag{7}$$

where J_{ii} is the i-th element of the Jacobian matrix

$$\mathbf{J} = \frac{\partial \mathbf{f}}{\partial \mathbf{c}} = \begin{bmatrix} \frac{\partial f_1}{\partial c_1} & \cdots & \frac{\partial f_1}{\partial c_n} \\ \vdots & \ddots & \vdots \\ \frac{\partial f_n}{\partial c_1} & \cdots & \frac{\partial f_n}{\partial c_n} \end{bmatrix} \tag{8}$$

Note that if species i has consuming reactions, the term J_{ii} is usually negative, since the derivative of the right-hand side of (1) with respect to the species itself has only negative terms. If i does not have any consuming reaction, then $J_{ii} = 0$. A slow variable can be defined as that who has a slow reactivity, i.e., a long lifetime

and, analogously, a fast variable is the one that reacts really fast, and therefore has a short lifetime [34].

Figure 1 shows the trajectory of species concentration over time for a fast (A) and slow (B) variable. When a slow variable undergo a perturbation, the distance between the perturbed and the original trajectories remains almost constant in time, whilst for the fast variable, the perturbed variable quickly approaches the original trajectory.

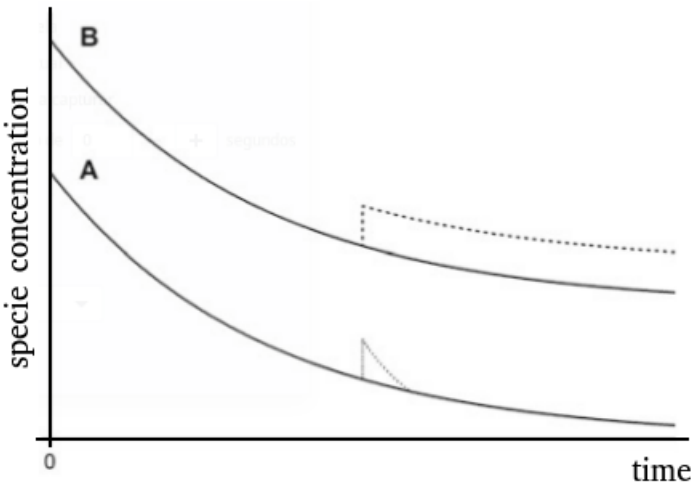

Fig. 1: Perturbed (dashed) and original trajectories for a fast (A) and slow (B) variable. Adapted from [34]

One important consideration is that the definition of slow or fast variable doesn't have relation with the magnitude of the production rate of the species. The separation in fast/slow variables depends on the system's response when there is a perturbation in the species concentration trajectory. The implication of this separation is that after the perturbation, fast variables can be determined by the slow variables values.

Changing the concentration of a species $\mathbf{c}$ during the path of oxidation in an arbitrary time $t_0 = 0$ according to the vector $\Delta\mathbf{c}^0$, one has the perturbed vector $\tilde{\mathbf{c}}$ given by

$$\tilde{\mathbf{c}}(0) = \mathbf{c}(0) + \Delta\mathbf{c}^0. \tag{9}$$

For a later time t, the perturbed vector is

$$\tilde{\mathbf{c}}(t) = \mathbf{c}(t) + \Delta\mathbf{c}. \tag{10}$$

Calculating the time derivative of the above expression, using linearisation and neglecting the high order terms of the Taylor expansion, one obtains

$$\begin{aligned} \frac{d}{dt}\tilde{\mathbf{c}}(t) &= \frac{d}{dt}\left(\mathbf{c}(t) + \Delta\mathbf{c}\right) \\ &\approx \mathbf{f}(\mathbf{c}, \mathbf{k}) + \frac{\partial \mathbf{f}}{\partial \mathbf{c}}\Delta\mathbf{c} \\ &= \mathbf{f}(\mathbf{c}, \mathbf{k}) + \mathbf{J}\Delta\mathbf{c}. \end{aligned} \tag{11}$$

Note that one can also express the derivative of (10) as a simple sum of the derivative, as

$$\frac{d}{dt}\tilde{\mathbf{c}}(t) \;=\; \frac{d}{dt}\left(\mathbf{c}(t)+\Delta\mathbf{c}\right) \;=\; \frac{d\mathbf{c}}{dt}+\frac{d\Delta\mathbf{c}}{dt}. \tag{12}$$

Comparing (11) and (12), the derivative of the perturbed concentration is equal to the product of the Jacobian and the perturbation itself, that is,

$$\frac{d\Delta\mathbf{c}(t)}{dt} \;=\; \mathbf{J}\Delta\mathbf{c}. \tag{13}$$

Although the Jacobian is time dependent, in a short time interval, it doesn't change significantly, so it can be considered constant. Therefore, Eq. (13) can be solved analytically:

$$\Delta\mathbf{c}(t) \;=\; \Delta\mathbf{c}^0\exp\left(\mathbf{J}t\right), \tag{14}$$

which represents the concentration change in the time t when there is a perturbation in time t_0. Supposing that $\mathbf{J}$ can be diagonalized, then

$$\mathbf{J} \;=\; \mathbf{W}^{-1}\Lambda\mathbf{W}, \tag{15}$$

where $\Lambda = \mathrm{diag}(\lambda_1,\ldots,\lambda_n)$, with λ_l the eigenvalues of $\mathbf{J}$. Substituting in Eq. (14),

$$\begin{aligned}\Delta\mathbf{c}(t) &= \Delta\mathbf{c}^0\exp\left(\mathbf{W}^{-1}\Lambda\mathbf{W}\right)\\ &= \Delta\mathbf{c}^0\mathbf{W}^{-1}\mathrm{diag}\left(e^{t\lambda_1},\ldots,e^{t\lambda_n}\right)\mathbf{W}\\ &= \Delta\mathbf{c}^0\sum_{l=1}^{n}e^{t\lambda_l}(v_l\cdot w_l^t),\end{aligned} \tag{16}$$

where v_l are the column-vectors of $\mathbf{W}^{-1}$ and w_l are the column-vectors of $\mathbf{W}$.

The analytical solution of (14) is a summation of exponential. Supposing that the eigenvalues have zero imaginary part, and since $\mathbf{J}$ is diagonalizable, the number of eigenvalues is equal to the number of variables of the system, and each eigenvalue is associated to a different time scale of the local linear solution of the system. This analysis is local due to setting the Jacobian constant.

The eigenvalue with the largest negative real part (i.e., more negative) correspond to a perturbation which decays very quickly, that is, represents the fastest time scale. However, it is not possible to make an one-to-one association of the eigenvalues with the variables (species concentrations), since for a system with several species coupling, different time scales can contribute to the consumption/production of each perturbed species trajectory.

According to these small perturbations of concentrations, lifetimes can be related to chemical kinetic systems. The lifetimes do not belong to a species, but to combinations of species concentrations defined by the left eigenvectors of the Jacobian [34]: the matrix $\mathbf{W}$. These left eigenvectors are called modes, and the vector $\mathbf{z}$ of

modes can be calculated as

$$\mathbf{z} \quad = \quad \mathbf{W}\mathbf{c}, \tag{17}$$

with the i-th mode coordinate given by

$$z_i \quad = \quad w_i \cdot \mathbf{c} \tag{18}$$

Therefore, concentrations can be calculated by

$$\mathbf{c} \quad = \quad \mathbf{W}^{-1}\mathbf{z} \; = \; \mathbf{V}\mathbf{z}, \tag{19}$$

or

$$c_i \quad = \quad v_i \cdot \mathbf{z}. \tag{20}$$

The change in time of the modes is given by the initial value problem, deduced from (1),

$$\begin{aligned} \frac{d\mathbf{c}}{dt} = \mathbf{f}(\mathbf{c},\mathbf{k}) \quad \Longrightarrow \quad & \frac{d\mathbf{V}\mathbf{z}}{dt} = \mathbf{f}(\mathbf{V}\mathbf{z},\mathbf{k}) \\ & \mathbf{V}\frac{d\mathbf{z}}{dt} = \mathbf{f}(\mathbf{V}\mathbf{z},\mathbf{k}) \\ & \frac{d\mathbf{z}}{dt} = \mathbf{V}^{-1}\cdot\mathbf{f}(\mathbf{V}\mathbf{z},\mathbf{k}) \\ & \frac{d\mathbf{z}}{dt} = \mathbf{W}\cdot\mathbf{f}(\mathbf{V}\mathbf{z},\mathbf{k}), \end{aligned} \tag{21}$$

with initial condition $\mathbf{z}_0 = \mathbf{W}\mathbf{c}_0$.

A perturbation in the concentration vector can be transferred to the modes using the relation

$$\Delta\mathbf{z} \quad = \quad \mathbf{W}\Delta\mathbf{c}. \tag{22}$$

With the ODE for the concentrations (13), a similar equation for $\mathbf{z}$ can be obtained

$$\begin{aligned} \mathbf{W}\frac{d\Delta\mathbf{c}}{dt} = \mathbf{W}\mathbf{J}\mathbf{V}\mathbf{W}\Delta\mathbf{c} \quad \Longrightarrow \quad & \mathbf{W}\frac{d\Delta\mathbf{c}}{dt} = \Lambda\mathbf{W}\Delta\mathbf{c} \\ & \frac{d}{dt}\left(\mathbf{W}\Delta\mathbf{c}\right) = \Lambda\Delta\mathbf{c} \\ & \frac{d\Delta\mathbf{c}}{dt} = \Lambda\Delta\mathbf{z}, \end{aligned} \tag{23}$$

whose analytical solution is

$$\Delta\mathbf{z} \quad = \quad \Delta\mathbf{c}_0 \exp\left(\Lambda t\right). \tag{24}$$

Since Λ is a diagonal matrix, the solution for each coordinate i of the modes is

$$\Delta z_i \quad = \quad \Delta z_i^0 e^{\lambda_i t}, \tag{25}$$

i.e., the perturbations in each of the modes are independent of each other.

The number of modes of the system is equal to the number of variables. Physically, the transformation matrix **W** shows how each species contributes to the modes associated with each eigenvalue. Ordering the eigenvalues, one can see which species are associated with the slow or fast modes of the system and therefore to identify those contributing with the fast modes (fast decay) and those contributing to the slower modes which may dominate the longer-term dynamics of the model.

The wide range of time scales in combustion is one of the reasons why chemical systems are computationally expensive to solve and stiff. Since very fast time scales are usually associated with local equilibrium processes, it is natural to base a method of mechanism reduction in some kind of time scale analysis [30]. It is often possible to separate and decouple these processes, and assume a local equilibrium with respect to the fastest time scales leading to a reduced set of equations. The next sections will describe the most common techniques of mechanism reduction based on time scale analysis.

2.1 Partial equilibrium hypothesis and quasi-steady-state assumption

The more straightforward and simple strategy in mechanism reduction is to identify and remove species and reactions that have negligible contributions to the phenomena of interest [22]. The traditional methodology for simplifying kinetics mechanism involve the use of the Quasi-Steady-State Assumption (QSSA) and/or the Partial Equilibrium approximation (PEA) [12]. This technique started to be used in the 1980s and continues to be employed as final step in mechanism reduction.

The QSSA is justified when the rates of production and destruction, in both forward and reverse reactions, of a number of species are much larger than the their net rate of formation. When applied to a species i, using Eq. (6), one sets $\dot{\omega}_i \approx 0$, and the following relation is obtained

$$0 \quad \approx \quad W_i \sum_{j=1}^{n_r} \nu_{kj} \left[k_{fj} \prod_{i=1}^{n_{sp}} [X_i]^{\nu'_{ij}} - k_{bj} \prod_{i=1}^{n_{sp}} [X_i]^{\nu''_{ij}} \right], \tag{26}$$

which can be used to estimate the concentration of a species as a function of the other species in the mechanism. This equality yields a system of algebraic relations among the elementary rates.

The PEA assumes that the forward and/or backward rates of some reactions are so large that they form a number of equilibria, expressed by an equal number of algebraic relations among the elementary reaction rates. Therefore, the forward and backward rates of certain reversible reactions are almost equal, such as the net rate is approximately zero, that is,

$$k_f \prod_{i=1}^{n_{sp}} [X_i]^{\nu'_i} \quad - \quad k_b \prod_{i=1}^{n_{sp}} [X_i]^{\nu''_i} = \dot{\omega} \approx 0 \tag{27}$$

$$k_f \prod_{i=1}^{n_{sp}} [X_i]^{\nu'_i} \quad \approx \quad k_b \prod_{i=1}^{n_{sp}} [X_i]^{\nu''_i} . \tag{28}$$

The algebraic relations obtained from QSSA and PEA is used to compute the concentration of species and to simplify the differential equations of the remaining species in the mechanism [12].

An important feature in QSSA is to choose which species are in steady-state. The following algorithm was proposed by Turányi *et al* [33]:

1. Firstly, the local error, associated with each species, of QSSA is calculated over the whole domain of the application;
2. A group of species to be in steady-state is selected following a user defined tolerence;
3. Local error is calculated for the group of species from step 2;
4. If the error remains low, the assumption is applied to the group of species from step 2. Otherwise, the tolerance is decreased.

Others techniques also can be used to find the species that are in QSSA, such as the level of importance index (LOI) [19] or the computational singular perturbation (see Section 2.2).

The use of QSSA and PEA methodologies is associated with the existence of dissipative times scales which are faster than the ones that characterize the long-term evolution of the system. Thus, separation of time scales are definitive to help chose the QSSA species or PEA reactions, since those are associated with the fast processes (equilibrium state).

2.2 Computational singular perturbation - CSP

The computational singular perturbation theory is a family of methods that uses variables transformation so that the time scales in complex chemistry systems can be separated. Lam e Goussis [15, 16, 17] developed a detailed theory based on the application of perturbation in species concentrations to find informations about the presence of QSSA species and PEA reactions inside a detailed mechanism, without any chemistry knownledge [30]. In other words, CSP helps to chose which species are in QSS and reactions in PE.

Consider a system with n variables. The eigenvalue analysis of the Jacobian provides n_f fast time scales, that is, eigenvalues with the largest negative real part. Then, the solution is quickly attracted to a surface Ω with dimension $(n-n_f)$, hereafter denominated slow manifold. Let $S_{\mathbf{c}}\Omega$ and $S_{\mathbf{c}}F$ be two subspaces of Ω, where the first is the space of trajectories in Ω and the latter the space containing the directions of fast approaches to the manifold. These subspaces are spanned by

$$S_{\mathbf{c}}\Omega = \text{span}\left(\mathbf{a}_i\right), i = n_f + 1, \ldots, n; \tag{29}$$

$$S_{\mathbf{c}}F = \text{span}\left(\mathbf{a}_i\right), i = 1, \ldots, n_f. \tag{30}$$

The vectors $\mathbf{a}_i$ are the eigenvectors of the Jacobian and form the columns of the matrices

$$\mathbf{A}_R = \begin{bmatrix} | & & | \\ \mathbf{a}_{n_f+1} & \ldots & \mathbf{a}_n \\ | & & | \end{bmatrix} \quad \text{and} \quad \mathbf{A}_S = \begin{bmatrix} | & & | \\ \mathbf{a}_1 & \ldots & \mathbf{a}_{n_f} \\ | & & | \end{bmatrix}. \tag{31}$$

In these basis, the right-hand side of Eq. (1) can be decomposed in

$$\mathbf{f}(\mathbf{c},\mathbf{k}) \quad = \quad \mathbf{f}_{\text{fast}}(\mathbf{c},\mathbf{k}) + \mathbf{f}_{\text{slow}}(\mathbf{c},\mathbf{k}), \tag{32}$$

where

$$\mathbf{f}_{\text{fast}} = \mathbf{A}_R \cdot \mathbf{z}^R \quad \text{and} \quad \mathbf{f}_{\text{slow}} = \mathbf{A}_S \cdot \mathbf{z}^S, \tag{33}$$

and $\mathbf{z}$ are the amplitudes defined by

$$\mathbf{z}^R = \mathbf{B}^R\mathbf{f} \quad \text{and} \quad \mathbf{z}^S = \mathbf{B}^S\mathbf{f}. \tag{34}$$

Vectors $\mathbf{b}^i$ are defined by $\mathbf{b}^i\mathbf{a}_j = \delta_i^j$.

When the trajectories reach the slow manifold, the fast time scales become exhausted and $\mathbf{f}$ has no components in the fast subspace $S_{\mathbf{c}}F$, and it is entirely in $S_{\mathbf{c}}\Omega$. Thus, the solution evolves inside Ω according to the slow time scales and the kinetics is governed by the equation

$$\frac{d\mathbf{c}}{dt} \quad \approx \quad \mathbf{f}_{\text{slow}}(\mathbf{c},\mathbf{k}). \tag{35}$$

The equation $\mathbf{z}^R \approx 0$ can be interpreted as a generalization of QSSA and PEA.

The advantage in using CSP is that a simple analysis of eigenvalues and eigenvectors of the system provides information about which species or reactions are associated with the fastest modes, although the computational cost of evaluating the Jacobian could be elevated.

2.3 Intrinsic Low Dimensional Manifolds

The concept of slow manifold introduced in the last section will provide a base for the theory of the intrinsic low dimensional manifolds (ILDM). The ILDM extracts the essential information of the full system to describe the most interesting and essential details of the system's chemical kinetics. It was developed by Maas and Pope [21] and allows to decouple the fast time-scales and globally reduce the dimension of the model. The main idea is to find a manifold of low dimension inside the vector space of thermochemical states (state space) that attracts the reactive processes.

As already explained, there is a difference in the time scales within a chemical system, which can be obtained via inspection of the eigenvalues of the Jacobian. Consider the local solution given by Eq. (16), describing the evolution of a perturbed chemical species. For each species, there is a summation of exponential, and each of these is associated with one time scale. Therefore, in general, all time scales affects the dynamics of each species, although the amount of how much each term affects a given species concentration is not the same for each species. Some species will evolve more quickly than the others for a initial period of time, i.e., governed by the fast time scales in this initial period. When enough time has passed, the slower time scales terms of the solutions begin to dominate the system and thus the evolution of each species concentration. This analysis yields the conclusion that the system behaviour is often contained in the terms correlated to the slower time

scales.

The summary is that as the trajectories of the concentrations evolve in the state space, the fast time scales will become exhausted. If a system has n_s slow time scales, the trajectories will approach a n_s-dimensional surface inside the state space, denominated low-dimensional manifold. If all time scales in the system become exhausted, an equilibrium chemical model arises, which represents a zero-dimensional manifold. This manifold is not characterized by any species concentrations, but by temperature and, in non-premixed flames, the mixture fraction, and the most usual example of this is the Burke-Schumann solution (mass fractions depending on mixture fraction). The low-dimensional manifold has the property to attract reaction trajectories, and the reaction path inside the detailed mechanism will approach the manifold rapidly, where the subsequently movement in the manifold will be slow. This slow movements in the manifolds are parametrized by the variables that it defines.

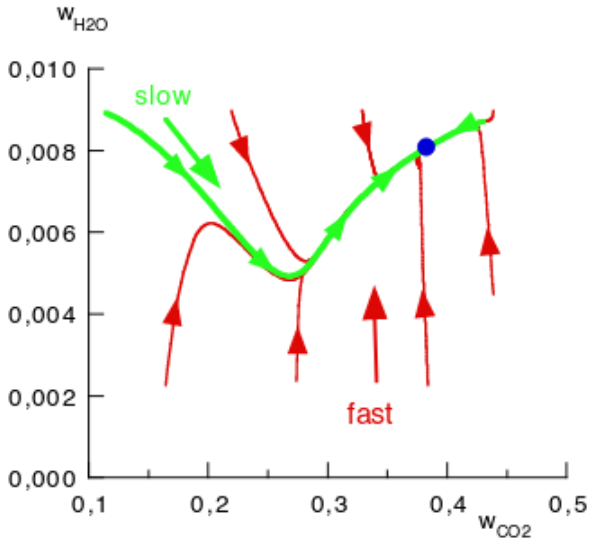

Fig. 2: Fast trajectories (red) approaching a slow surface (green) in the 2D state space.

The question addressed in the precursor work of Maas and Pope was that [21]: If there is a low-dimensional attracting manifold in the state space with the property that if a trajectory is near the manifold, it will remain close to it for all times? And if so, can it be used to provide a simplified model of chemical kinetics? The answer for this question is affirmative, and the theory is the ILDM, presented below.

Consider a homogeneous, isobaric and adiabatic chemical reaction system with n_{sp} species given by

$$\frac{\partial h}{\partial t} = 0 \tag{36}$$

$$\frac{\partial p}{\partial t} = 0 \tag{37}$$

$$\frac{\partial \phi_i}{\partial t} = \dot{\omega}_i, \qquad i = 1, \ldots n_{sp}, \tag{38}$$

where h is the enthalpy, p the pressure and ϕ_i the specific mole fraction ($\phi = Y_i/W_i$) of species i. This system

is often written in terms of vectors, i.e.,

$$\frac{\partial \mathbf{\Psi}}{\partial t} = \mathbf{F}(\mathbf{\Psi}), \tag{39}$$

where $\mathbf{\Psi} = \left(h, p, \phi_i, \ldots, \phi_{n_{sp}}\right)^T$ and $\mathbf{F} = \left(0, 0, f_1, \ldots, f_{n_{sp}}\right)^T$ are n-dimensional vectors ($n = n_{sp} + 2$).

For each point in the state space, the eigenvalues of the Jacobian matrix ($\mathbf{F}_{\mathbf{\Psi}}$) are calculated to identify the n time scales of the system. The corresponding eigenvectors describe the characteristic directions associated with those time scales. The general idea is to look for points in the state space for which components in the direction of certain eigenvectors, those associated with fast time scales, vanishes.

Generally, the eigenvectors provided by diagonalization are not orthogonal, and the elimination of characteristic directions associated with fast time scales are more easily carried out when the directions associated with each time scale are orthogonal [26]. Therefore, one way to accomplish that is using the Schur decomposition of the Jacobian at each point of the state space, that is,

$$\mathbf{Q}^T \mathbf{F}_{\mathbf{\Psi}} \mathbf{Q} = N, \tag{40}$$

where the eigenvalues λ_i of the Jacobian appear in the diagonal of the upper triangular matrix N in the order of descending real parts [21]. For chemical systems, the Jacobian contain real numbers and it has been proved that the Schur decomposition always exists for a matrix whose elements are real [10]. Matrix $\mathbf{Q}$ is orthonormal, and its vector columns provides the desired orthogonal set of directions in the state space associated with fast time scales.

Thus, supposing that the Schur decomposition exists for every point in the solution space, a n_l-dimensional manifold ($n_l < n$) is obtained, whose points are calculated by

$$\mathbf{Q}_L^T(\mathbf{\Psi}) \cdot \mathbf{F}(\mathbf{\Psi}) = 0 \tag{41}$$

where $\mathbf{Q}_L^T(\mathbf{\Psi})$ is a $n_f \times n$ matrix ($n_f = n - n_l$). Equation (41) is called ILDM equation, and the matrix $\mathbf{Q}_L^T$ is obtained by eliminating the n_l first rows of $\mathbf{Q}^T$, namely, the rows that correspond to the conserved and slowly changing variables.

One problem arising from Eq. (41) is that the system is not closed. There are other n_l additional parameters equations necessary to complete the equation system. These new equations will affect the uniqueness and existence of the manifold, but not the construction of the manifold itself [21]. Thus, to identify the low-dimensional manifold, the following system has to be solved

$$\begin{bmatrix} \mathbf{Q}_L^T(\mathbf{\Psi}) \cdot \mathbf{F}(\mathbf{\Psi}) \\ \mathbf{P}(\mathbf{\Psi}, \tau) \end{bmatrix} = 0, \tag{42}$$

with $\mathbf{P}(\mathbf{\Psi}, \tau)$ being the n_l additional parameters equations.

A proper numerical scheme should be used to solve Eq. (42), such as the Newton's method. The ILDM gives an accurate description if the application is not required at extremely small times. Thus, in regions of low temperatures, the ILDM is not well predicted. For instance, ignition delay times calculation, since for

this processes, the phenomena occurs very quickly within a low temperature region. Another drawback is that ILDM does not consider the transport processes. One alternative for this is the Reaction Diffusion Manifold technique, exploited in Section 4.

3 Flamelet concept

The flamelet concept is briefly discussed here since consist in a very good approximation for the REDIM, and is tightly close to the counterflow configuration. It was first introduced by Peters [23] for non-premixed turbulent combustion, and consists in a variety of physical models in which the turbulent flame is viewed as a collection of laminar flame elements embedded in a turbulent flow and interacting with it. The main advantage of the flamelet concept is that decouples the complex chemical structure of the flame from the fluid dynamics, which can be modeled independently [8].

For a non-premixed flame, the local structure of the flame in each point of the flame front (i.e., the surface where $\xi(t, \mathbf{x}) = \xi_{st}$), is defined by a laminar flamelet. Using the transformation $(t, \mathbf{x}) \rightarrow (t, \xi)$, the coordinate system becomes the flame front and the physical space is transformed to a mixture fraction space where the only independent variable is ξ [7]. The unsteady equations for temperature and mass fractions, respectively, are therefore given by

$$\rho \frac{\partial w_i}{\partial t} = \frac{\rho \chi}{2Le_i} \frac{\partial^2 w_i}{\partial \xi^2} + \dot{\omega}_i \tag{43}$$

$$\rho \frac{\partial T}{\partial t} = \frac{\rho \chi}{2} \frac{\partial^2 T}{\partial \xi^2} - \frac{1}{c_p} \left(\sum_{i=1}^{n_{sp}} h_i \dot{\omega}_i - Q_R \right). \tag{44}$$

The scalar dissipation rate χ is given by

$$\chi = 2D_\xi \left(\nabla \xi \cdot \nabla \xi \right). \tag{45}$$

The instantaneous scalar dissipation rate consists a very important characteristic in non-premixed combustion, specially χ in stoichiometric conditions, χ_{st}, which denotes how far the flame is from the equilibrium point [7]. Since diffusion fluxes arising from spatial gradients are described as function of the mixture fraction gradients [25], the influence of the flow field on the flamelet structure is completely described by χ. Also, χ can be interpreted as the inverse of the characteristic diffusion time [24]. Thus, the higher is χ, the lower is the characteristic diffusion time scale, and consequently the lower is the Damköhler number. It is straightforward then that if $\chi = 0$, the flamelet concept becomes the Burke-Schumann solution.

The solution for a non-premixed flame is therefore calculated solving the fluid dynamic equations and the mixture fraction. Nevertheless, a key difficult in integrating Eqs. (43) and (44) is to know a priori informations of the scalar dissipation rate dependence of the mixture fraction. Thus, flamelet libraries are usually computed in advance in a pre-processing step, totally independent of the flow. Generally, those libraries are built using counterflow non-premixed flames solutions with detailed chemistry.

If chemistry is considered infinitely fast, the time derivative in the flamelet equations (43) and (44) vanishes. An important condition for the flamelet approach is that the flame thickness is sufficiently small compared to

the length scales [8]. The great advantage of the flamelet compared to the flame sheet model is that it doesn't need to imply hypothesis to the reaction rates and so complete detailed mechanisms can be used.

For a given steady solution, the flamelet equations define an one dimensional manifold in the state space, parametrized by the mixture fraction, that is, all the thermodynamic properties are functions only of the mixture fractions ξ [13]. That is the great disadvantage of this method, since the reactive scalars are constant throughout the iso-surfaces of the mixture fraction. Nevertheless, several methods for chemistry modeling were developed using the flamelet approach, the best know being the flamelet generated manifold (FGM) [35] which combines the idea of flamelet and slow manifolds, and is used in the commercial CFD code FLUENT.

4 Reaction diffusion manifolds - REDIM

The ideas exploited for building the ILDM in Section 2.3 regarding the separation of time scales will be used to develop the theory of Reaction Diffusion Manifolds - REDIM. This technique is an improvement of the ILDM, since takes into account the transport processes, and not only reaction. It will be shown that the thermodynamic states of the system evolves towards a low dimensional manifold, that can be calculated using the diffusion and reaction terms of the equation of the variables, such as convection is not necessary.

The time scales separation which leads to the idea that the system dynamics approach a slow manifold in the space states so that all thermodynamic variables can be predicted as a function of the ones that parametrizes the manifold is extended for diffusion and convection systems. Evolution in time of the thermodynamics properties consists of a reaction, a convection and a diffusion term. The major drawback of the ILDM technique is that, since the diffusive/convective terms of the equations are dominant in the pre-heat zones, that is, the zone before ignition, using only the reaction term, this area of the state space is not covered.

The first attempt of overcoming this problem was developed by Bykov and Maas [4], which suggested a procedure to use ILDM in the whole domain of the state space. They subdivided the domain of interest in three different sub-domains: in the first one, only the chemical kinetic governs the system dynamics; in the second, chemical and convection/diffusion processes are strongly coupled and the third one, where an infinitly slow chemstry assumption is used so that the reaction term is neglected and the system dynamics is governed only by convection/diffusion. The domais were treated separately and three different slow manifolds were obtained. Nevertheless, this approach also had some problems, due to the assumption that the second domain asymptotically shrinks into the boundary between the first and third domain.

The REDIM technique was later introduced also by Bykov and Maas in 2007 [3], whose used the invariant condition to obtain the slow manifold in the state space. This hypothesis were very useful since provided the basic assumption for developing the REDIM equation. The dimension of the REDIM can be choose depending on the complexity of the combustion process to be modeled, and it has been proved that the 1D-REDIM is equivalent to the flamelet concept [3, 14], while 2D and 3D-REDIM are sufficient to calculate complex chemistry calculations, such as turbulent three dimensional flames.

From a numerical point of view, the advantage of using a method where the system is governed only by the slow time scales is in the fact that one can use higher time steps in the numerical schemes, decreasing the stiffness of the system. The next section will introduce the concept of invariant manifolds so that later the

REDIM equation can be developed.

4.1 The invariance condition

The thermochemical state in a reactive system with n_{sp} species can be described by the $n = n_{sp} + 2$ dimension vector

$$\mathbf{\Psi} = \left(h, p, \phi_1, \ldots, \phi_{n_{sp}}\right), \tag{46}$$

where h is the specific enthalpy, p the pressure and ϕ_i is the specific mole fraction of species i, defined as $\phi_i = w_i/W_i$. The thermochemical state changes over chemical and transport processes due the PDE, in vector notation, [3]

$$\frac{\partial \mathbf{\Psi}}{\partial t} = \mathbf{F}(\mathbf{\Psi}) - \mathbf{u} \cdot \mathbf{grad}(\mathbf{\Psi}) - \frac{1}{\rho}\mathbf{div}\left(\mathbf{D} \cdot \mathbf{grad}(\mathbf{\Psi})\right) = \mathbf{\Phi}(\mathbf{\Psi}) \tag{47}$$

Here, $\mathbf{u}$ is the velocity, $\mathbf{D}$ is the $n \times n$ diffusion matrix, $\mathbf{F}$ is the n-dimensional source term that accounts for the chemical reactions and ρ the density. The second term of the right-hand side in Eq. (47) represents convection and the third term diffusion.

After the fast time scales are exhausted, the system dynamics is governed by the m_s slowest modes ($m_s < n$), i.e., the system solution is within a m_s-dimensional manifold in the state space. This manifold $\mathcal{M}$ is defined as

$$\mathcal{M} = \left\{\mathbf{\Psi} : \mathbf{\Psi} = \mathbf{\Psi}(\boldsymbol{\theta}), \mathbf{\Psi} : \mathbb{R}^{m_s} \to \mathbb{R}^n\right\}, \tag{48}$$

where $\boldsymbol{\theta}$ is the m_s-dimensional vector that parametrizes the manifold. The explicit function $\mathbf{\Psi}(\boldsymbol{\theta})$ defines a surface in $\mathbb{R}^n$ with dimension m_s.

The manifold $\mathcal{M}$ is said invariant if, and only if, for some θ_*, such that $\mathbf{\Psi}(\theta_*) \in \mathcal{M}$, then for all $\theta > \theta_*$, $\mathbf{\Psi}(\theta) \in \mathcal{M}$ (this definition can be found in Gorban and Karlin [11]). The consequence of this definition is that for every $\mathbf{\Psi} \in \mathcal{M}$, it holds that $\mathbf{\Phi}(\mathbf{\Psi}) \in T_\Psi \mathcal{M}$, that is, the field $\mathbf{\Phi}$ (defined by the right-hand side of Eq. (47)) applied to the vectors of the manifold belong to the tangent space of $\mathcal{M}$. To exemplify this, lets consider a two dimensional system with only the reaction term, that is,

$$\frac{\partial \mathbf{\Psi}}{\partial t} = \mathbf{F}(\mathbf{\Psi}). \tag{49}$$

In this case, the invariant manifold $\mathcal{M}$ will have dimension equal to one. In the point $\theta_* \in \mathcal{M}$, the derivative of $\mathbf{\Psi}$ in this point is equal to

$$\left.\frac{\partial \Psi}{\partial t}\right|_{\theta=\theta_*} = \mathbf{F}(\mathbf{\Psi}(\theta_*)) \tag{50}$$

Considering that for every point θ in the manifold, $\mathbf{F}(\mathbf{\Psi}(\theta)) \in \mathcal{M}$, the derivative of $\mathbf{\Psi}$ in the point θ_* will belong to the manifold, and, since this derivative is equal to the field $\mathbf{F}$ applied in the vector, and also since this will hold for every $\theta > \theta_*$, it can be concluded that, for the points within the manifold, $\mathbf{F}(\mathbf{\Psi}(\theta)) \in T_\Psi \mathcal{M}$.

The generalization of this for the filed $\mathbf{\Phi}$ follows analogously.

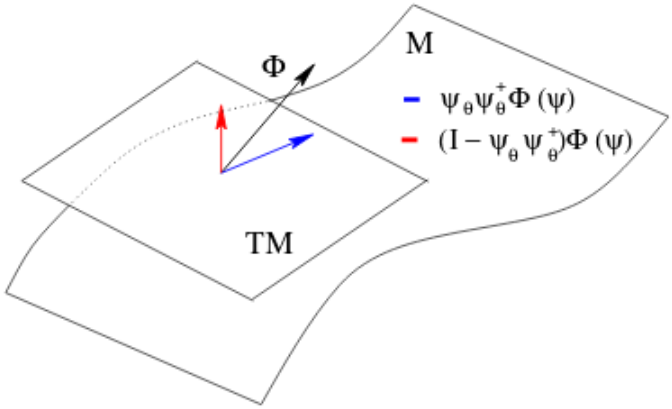

Fig. 3: The invariance condition: $\mathbf{\Phi}(\mathbf{\Psi})$ belongs to the tangent space of the manifold, it follows that it is orthogonal to the normal space of $\mathcal{M}$.

Therefore, as $\mathbf{\Phi}(\mathbf{\Psi})$ belongs to the tangent space of the manifold, it follows that it is orthogonal to the normal space of $\mathcal{M}$. This implies that

$$(\mathbf{\Psi}_{\boldsymbol{\theta}}^{\perp}(\boldsymbol{\theta}))^T \cdot \mathbf{\Phi}(\mathbf{\Psi}) \quad = \quad 0, \tag{51}$$

for all $\boldsymbol{\theta}$. Here, $\mathbf{\Psi}_{\boldsymbol{\theta}}^{\perp}$ represents the normal space of $\mathcal{M}$, i.e.,

$$(\mathbf{\Psi}_{\boldsymbol{\theta}}^{\perp})^T \cdot \mathbf{\Psi}_{\boldsymbol{\theta}} \quad = \quad 0. \tag{52}$$

The condition (51) implies that the projection of the field $\mathbf{\Phi}$ in the normal space of $\mathcal{M}$ is also orthogonal to the field, that is,

$$P_{(T\mathcal{M})^\perp}\left[\mathbf{\Phi}(\mathbf{\Psi})\right] \cdot \mathbf{\Phi}(\mathbf{\Psi}) \quad = \quad 0 \tag{53}$$

But,

$$P_{(T\mathcal{M})^\perp}\left[\mathbf{\Phi}(\mathbf{\Psi})\right] \quad = \quad \left(\mathbf{\Psi}_{\boldsymbol{\theta}}^{\perp}(\boldsymbol{\theta}) \cdot \mathbf{\Psi}_{\boldsymbol{\theta}}^{+}(\boldsymbol{\theta})\right) \cdot \mathbf{\Phi}(\mathbf{\Psi}) \tag{54}$$

where $\mathbf{\Psi}_{\boldsymbol{\theta}}^{+}$ is the Moore-Penrose pseudo-inverse, defined by

$$\mathbf{\Psi}_{\boldsymbol{\theta}}^{+} \quad = \quad \left(\mathbf{\Psi}_{\boldsymbol{\theta}}^T \cdot \mathbf{\Psi}_{\boldsymbol{\theta}}\right)^{-1} \cdot \mathbf{\Psi}_{\boldsymbol{\theta}}^T. \tag{55}$$

This pseudo-inverse always exists when the columns of $\mathbf{\Psi}_{\boldsymbol{\theta}}$ are linearly independent (i.e., the matrix $\mathbf{\Psi}_{\boldsymbol{\theta}}^T \cdot \mathbf{\Psi}_{\boldsymbol{\theta}}$ is non-singular). This can always be achieved by a suitable choice of the local coordinates $\boldsymbol{\theta}$. Then, using (54) in

(53), one obtains

$$\begin{aligned} P_{(T\mathcal{M})^\perp}\left[\boldsymbol{\Phi}(\boldsymbol{\Psi})\right]\cdot\boldsymbol{\Phi}(\boldsymbol{\Psi}) &= \left[\left(\boldsymbol{\Psi}_{\boldsymbol{\theta}}^{\perp}(\boldsymbol{\theta})\cdot\boldsymbol{\Psi}_{\boldsymbol{\theta}}^{+}(\boldsymbol{\theta})\right)\cdot\boldsymbol{\Phi}\left(\boldsymbol{\Psi}(\boldsymbol{\theta})\right)\right]\cdot\boldsymbol{\Phi}\left(\boldsymbol{\Psi}(\boldsymbol{\theta})\right) \\ &= \left(I-\boldsymbol{\Psi}_{\boldsymbol{\theta}}(\boldsymbol{\theta})\cdot\boldsymbol{\Psi}_{\boldsymbol{\theta}}^{+}(\boldsymbol{\theta})\right)\cdot\boldsymbol{\Phi}\left(\boldsymbol{\Psi}(\boldsymbol{\theta})\right). \end{aligned} \tag{56}$$

Hence,

$$\left(I-\boldsymbol{\Psi}_{\boldsymbol{\theta}}(\boldsymbol{\theta})\cdot\boldsymbol{\Psi}_{\boldsymbol{\theta}}^{+}(\boldsymbol{\theta})\right)\cdot\boldsymbol{\Phi}\left(\boldsymbol{\Psi}(\boldsymbol{\theta})\right) = 0. \tag{57}$$

The relation (57) is very important in the REDIM formulation since allows to simplify Eq. (47) and to find an approximation for the low-dimensional manifold [3]. Nevertheless, to solve (57), two difficulties arise [14]: first, the dependence of $\boldsymbol{\Psi}\in\mathcal{M}$ as a function of the local coordinates $\boldsymbol{\theta}$ should be explicitly determined and second, $\boldsymbol{\Phi}(\boldsymbol{\Psi}(\boldsymbol{\theta}))$ depends on the spatial gradients of $\boldsymbol{\theta}$, i.e., the transport processes, that cannot be known *a priori*. In the next section, these difficulties will be discussed.

4.2 REDIM equation

To solve the difficulties highlighted in last section, the right-hand side of Eq. (47) has to be analysed. First, observe that

$$\mathbf{grad}(\boldsymbol{\Psi}(\boldsymbol{\theta})) = \begin{pmatrix} \sum_{k=1}^{m_s}\frac{\partial\Psi_1}{\partial\theta_k}\frac{\partial\theta_k}{\partial x_k} \\ \vdots \\ \sum_{k=1}^{m_s}\frac{\partial\Psi_n}{\partial\theta_k}\frac{\partial\theta_k}{\partial x_k} \end{pmatrix} \tag{58}$$

$$= \begin{pmatrix} \frac{\partial\Psi_1}{\partial\theta_1} & \cdots & \frac{\partial\Psi_1}{\partial\theta_{m_s}} \\ \vdots & \ddots & \vdots \\ \frac{\partial\Psi_n}{\partial\theta_1} & \cdots & \frac{\partial\Psi_n}{\partial\theta_{m_s}} \end{pmatrix} \begin{pmatrix} \frac{\partial\theta_1}{\partial x_1} \\ \vdots \\ \frac{\partial\theta_{m_s}}{\partial x_j} \end{pmatrix} \tag{59}$$

$$= \boldsymbol{\Psi}_{\boldsymbol{\theta}}\mathbf{grad}(\theta) \tag{60}$$

Thus, the convective term of Eq. (47) reads

$$\mathbf{u}\cdot\mathbf{grad}(\boldsymbol{\Psi}) = \mathbf{u}\cdot\left(\boldsymbol{\Psi}_{\boldsymbol{\theta}}\mathbf{grad}(\theta)\right). \tag{61}$$

The diffusive term in Eq. (47) is rearranged as [13]:

$$\begin{aligned}
\frac{1}{\rho}\mathbf{div}\left(\mathbf{D}\cdot\mathbf{grad}(\mathbf{\Psi})\right) &= \frac{1}{\rho}\mathbf{div}\left[\mathbf{D}\cdot(\mathbf{\Psi_\theta}\mathbf{grad}(\theta))\right] \\
&= \frac{1}{\rho}\sum_{i=1}^{3}\frac{\partial}{\partial x_i}\left(\sum_{j=1}^{n}\sum_{k=1}^{m_s}D_j\frac{\partial\Psi_j}{\partial\theta_k}\frac{\partial\theta_k}{\partial x_i}\right) \\
&= \frac{1}{\rho}\sum_{i=1}^{3}\sum_{j=1}^{n}\sum_{k=1}^{m_s}\left[\frac{\partial}{\partial x_i}\left(D_j\frac{\partial\Psi_j}{\partial\theta_k}\right)\frac{\partial\theta_k}{\partial x_i}+D_j\frac{\partial\Psi_j}{\partial\theta_k}\frac{\partial}{\partial x_i}\frac{\partial\theta_k}{\partial x_i}\right] \\
&= \frac{1}{\rho}\sum_{i=1}^{3}\sum_{j=1}^{n}\sum_{k=1}^{m_s}\left[\sum_{h=1}^{m_s}\frac{\partial}{\partial\theta_h}\left(D_j\frac{\partial\Psi_j}{\partial\theta_k}\right)\frac{\partial\theta_h}{\partial x_i}\frac{\partial\theta_k}{\partial x_i}+D_j\frac{\partial\Psi_j}{\partial\theta_k}\frac{\partial}{\partial x_i}\frac{\partial\theta_k}{\partial x_i}\right] \\
&= \frac{1}{\rho}\left[(\mathbf{D}\cdot\mathbf{\Psi}_\theta)_\theta\circ\mathbf{grad}(\theta)\circ\mathbf{grad}(\theta)+(\mathbf{D}\cdot\mathbf{\Psi}_\theta)\cdot\mathbf{div}(\mathbf{grad}(\theta))\right].
\end{aligned}$$

Equation (47) becomes

$$\begin{aligned}
\frac{\partial\mathbf{\Psi}}{\partial t}=\mathbf{F}(\mathbf{\Psi})-\mathbf{u}\cdot(\mathbf{\Psi_\theta}\mathbf{grad}(\theta)) &- \frac{1}{\rho}\left[(\mathbf{D}\cdot\mathbf{\Psi}_\theta)_\theta\circ\mathbf{grad}(\theta)\circ\mathbf{grad}(\theta)\right. \\
&+ \left.(\mathbf{D}\cdot\mathbf{\Psi}_\theta)\cdot\mathbf{div}(\mathbf{grad}(\theta))\right]. \qquad (62)
\end{aligned}$$

For simplicity, two hypothesis will be assumed: the Lewis number equal to unity and equal diffusivities for all species, so that the diffusion matrix $\mathbf{D}$ is given by $\mathbf{D}=d\cdot I$. These hypothesis are very common in numerical simulations of combustion processes. Applying the projection operator of Eq. (62) to each term of Eq. (47), some simplifications can be made. For instance,

$$\begin{aligned}
\left(I-\mathbf{\Psi_\theta}(\boldsymbol{\theta})\cdot\mathbf{\Psi_\theta^+}(\boldsymbol{\theta})\right)\cdot(\mathbf{u}\cdot(\mathbf{\Psi_\theta}\mathbf{grad}(\theta))) &= \mathbf{u}\cdot(\mathbf{\Psi_\theta}\mathbf{grad}(\theta)) \\
&- \underbrace{\mathbf{\Psi_\theta^+}(\boldsymbol{\theta})\cdot\mathbf{\Psi_\theta}(\boldsymbol{\theta})}_{=\ I}\mathbf{u}\cdot(\mathbf{\Psi_\theta}\mathbf{grad}(\theta)) \\
&= \mathbf{u}\cdot(\mathbf{\Psi_\theta}\mathbf{grad}(\theta))-\mathbf{u}\cdot(\mathbf{\Psi_\theta}\mathbf{grad}(\theta)) \\
&= 0 \qquad (63)
\end{aligned}$$

This proves that the convection term vanishes in the invariant manifold. Also, it is valid that

$$\begin{aligned}
\left(I-\mathbf{\Psi_\theta}(\boldsymbol{\theta})\cdot\mathbf{\Psi_\theta^+}(\boldsymbol{\theta})\right) &\cdot [(d\cdot\mathbf{\Psi}_\theta)\cdot\mathbf{div}(\mathbf{grad}(\theta))] \\
&= d\left[\mathbf{\Psi}_\theta\cdot\mathbf{div}(\mathbf{grad}(\theta))-\mathbf{\Psi_\theta}(\boldsymbol{\theta})\cdot\underbrace{\mathbf{\Psi_\theta^+}(\boldsymbol{\theta})\mathbf{\Psi}_\theta}_{=\ I}\cdot\mathbf{div}(\mathbf{grad}(\theta))\right] \\
&= d\left[\mathbf{\Psi}_\theta\cdot\mathbf{div}(\mathbf{grad}(\theta))-\mathbf{\Psi}_\theta\cdot\mathbf{div}(\mathbf{grad}(\theta))\right] \\
&= 0 \qquad (64)
\end{aligned}$$

Therefore, using the relation given in (57), one obtains that

$$\left(I-\mathbf{\Psi_\theta}(\boldsymbol{\theta})\cdot\mathbf{\Psi_\theta^+}(\boldsymbol{\theta})\right)\cdot\left[\mathbf{F}(\mathbf{\Psi})-\frac{d}{\rho}\mathbf{\Psi}_{\theta\theta}\circ\mathbf{grad}(\theta)\circ\mathbf{grad}(\theta)\right] = 0 \qquad (65)$$

The relation above implies that if the equality is fulfilled, then the vector $\mathbf{\Psi}(\theta)$ is in the reduced manifold within the state space. Besides, it is important that the spatial dependence of the gradient of θ can be eliminated, that is, $\mathbf{grad}(\theta) = f(\theta)$. To obtain a numerical solution of Eq. (65), the strategy proposed by Bykov and Maas was to reformulate the equation into a system of parabolic PDEs, with appropriate boundary and initial conditions. Thus, the REDIM equations read [3]

$$\begin{cases} \dfrac{\partial \mathbf{\Psi}(\theta)}{\partial t} = \left(I - \mathbf{\Psi_{\theta}}(\boldsymbol{\theta}) \cdot \mathbf{\Psi}^{+}_{\boldsymbol{\theta}}(\boldsymbol{\theta})\right) \cdot \left[\mathbf{F}(\mathbf{\Psi}) - \dfrac{d}{\rho}\mathbf{\Psi}_{\theta\theta} \circ \mathbf{grad}(\theta) \circ \mathbf{grad}(\theta)\right]; \\ \mathbf{\Psi}^{0} = \mathbf{\Psi}^{\text{init}}(\theta), \end{cases} \tag{66}$$

where $\mathbf{\Psi}^{\text{init}}$ is an initial guess for the reduced manifold. The stationary solution $\mathbf{\Psi}(\theta, \infty)$ given by Eq. (66) yields the desired reduced manifold. To integrate the REDIM equation until it converges, it is necessary to approximate the gradient of θ and to define a good initial guess for the starting manifold.

In the precursor work of Bykov and Maas [3], the dependence of the local gradients were studied for a two dimensional system, in order that the reduced manifold have one dimension. Four different cases were studied for the gradients:

(i) The exact gradients, obtained from a detailed simulation: $\mathbf{grad}(\theta) = \mathbf{grad}_{\text{exact}}(\theta)$;

(ii) the maximum value of the exact gradients calculated in (i): $\mathbf{grad}(\theta) = \max\left(\mathbf{grad}_{\text{exact}}(\theta)\right)$;

(iii) one order of magnitude less than (ii): $\mathbf{grad}(\theta) = 0.1\max\left(\mathbf{grad}_{\text{exact}}(\theta)\right)$;

(iv) one order of magnitude higher than (ii): $\mathbf{grad}(\theta) = 10\max\left(\mathbf{grad}_{\text{exact}}(\theta)\right)$.

As expected, the best results were for the gradients obtained from a detailed simulation, while the third and fourth cases above produced the worst results. It is worth noting that the one-dimensional REDIM built in this example using exact gradients is equivalent to the flamelet approach. By the observations, it was possible to conclude that the low dimensional manifolds are not very sensitive to the local coordinate gradients. As a comparison with the FGM method, the problem of estimating the gradients in REDIM is comparable with defining the scalar dissipation rate χ.

Another issue that is important when solving the system (66) is the choice of parametrization, i.e. defining the parameters for the vector θ. Albeit it does not affects the manifold itself (the manifold is independent of the parametrization), it affects the existence and the uniqueness of the REDIM equation (66). There is no physical motivation for the parametrization, which can be done using temperature, enthalpy, specific mole fractions of species or elements, species concentrations or even a combination of these.

It is generally a good strategy to define, for a 2D-REDIM, one variable accounting for mixture progress and another for reaction progress. For instance, the solution of a methane/air flame is provided in Fig. 4. It can be observed that $\theta_1 = N_2$ and $\theta_2 = CO_2$ are a good choice for parametrization, since the projection of the solution in this space is well defined. However, if one chooses for the same simulation $\theta_1 = CO_2$ and $\theta_2 = H_2O$ as parametrization, the monotonic behaviour of the solution is lost and thus the uniqueness of the solution.

Several types of parametrization and gradients estimatives has been observed in the literature. For instance, in the work of Steinhilber and Maas [29], for a premixed lean methane turbulent flame, the 2D-REDIM was

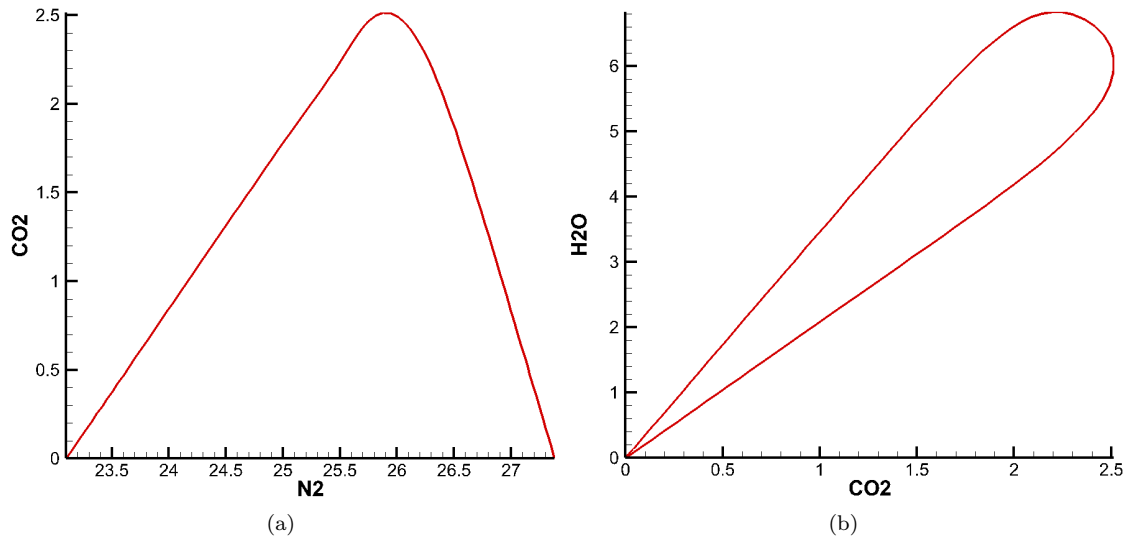

(a) (b)

Fig. 4: Solution of a counterflow non-premixed flame projected in (a) $\theta_1 = N_2$ and $\theta_2 = CO_2$ plane and (b) $\theta_1 = CO_2$ and $\theta_2 = H_2O$ as parametrization. It is clear that the uniqueness of solution in the second case is lost.

used with $\theta_1 = N_2$ and $\theta_2 = CO_2$ as parametrization. For the gradients, two one-dimensional simulations were performed. For the nitrogen, it was estimated a constant value of $\mathbf{grad}(N_2) = -500\ mol/kg.m$, through solution of a counterflow flame with same boundary and initial conditions that the turbulent flame to be simulated. For the carbon dioxide, the gradients were obtained using a detailed premixed flat flame.

The work of Fischer *et al.* [9], PDF simulations were performed to analyse the ignition of free turbulent jets of propane, ethylene and hydrogen. A 2D-REDIM was built and the parametrization variables were the enthalpy and, for hydrogen, the specific mole fraction of H_2O and for the hydrocarbons, the specific mole fraction of CO_2. A counterflow scheme with detailed chemistry were used to provide the gradients estimative.

In the works of Wang *et al.* [36, 37], large eddy simulation with filtered density functions were used with REDIM to simulate turbulent flames. In the first work, a 1D-REDIM was used with CO_2 as parametrization, since the simulation considered a fully premixed methane/air flame with constant equivalence ratio and without local extinction phenomena. The second work uses a 2D-REDIM with N_2 and CO_2 as parametrization of the manifold to study the local extinction and re-ignition of two lean premixed piloted natural gas/air flames. Schiessl *et al.* [28] used a direct numerical simulation (DNS) of a non-premixed turbulent planar flame of H_2 and air to obtain the gradients for the REDIM equation to study multi-directional molecular diffusion.

It is concluded by the literature that a good choice for parametrization of a 2D-REDIM is nitrogen and carbon dioxide. The fact that N_2 remains almost unchanged in the evolution of the system makes it a good choice to account for mixture progress, in the role of a conserved scalar. The CO_2 is a good choice for reaction progress since generally its quantity is large compared to all others species. Also, the estimative of the gradients provided by detailed one dimensional simulations is the best choice.

The gradient estimative and the parametrization helps to solve Eq. (66). Nevertheless, a suitable choice for the initial guess of the manifold is a crucial point to obtain a good (and fast) converged solution. Next section will treat with initial and boundary conditions for the REDIM equation.

4.3 Initial and boundary conditions

The REDIM is independent of initial condition's choice. This is clear since, as mentioned in section 2.3, as the fast time scales are dumped, the system dynamics will always approach the equilibrium point. This means also that for any starting point, the state will achieve the slow manifold. It is understood here that the initial and boundaries conditions will form the initial guess for integration of Eq. (66).

Nonetheless, since Eq. (66) denotes a stiff system of PDEs, a suitable choice for the initial condition avoid numerical instabilities and speed up the convergence. For instance, the extended ILDM, which represents the limiting case where the reaction term $\mathbf{F}(\mathbf{\Psi})$ is dominant and the transport processes can be neglected, can be used as initial condition. In this matter, the reaction curve can also be used.

Generally, one-dimensional simulations with detailed chemistry can provide a good initial condition for the REDIM equation. As already mentioned, since the 1D-REDIM is equivalent to the flamelet technique, it seems proper to use a flamelet with same boundary conditions (defined by the unburned mixtures) as initial condition for 1D-REDIM.

For a 2D-REDIM, several flamelets with the same conditions for the unburned mixtures can be computed and used to form the initial guess. The only drawback here is to define the boundary of the manifold, since the unburned mixtures do not provide conditions for all the boundary [13].

One strategy would be to take the flamelets with different strain rates, to cover the domain from stable flames until the extinction limit. As explained by Bykov *et al.* [6], the flamelet approach used for the initial guess represents a stationary solution set of detailed systems that are theoretically close to the REDIM for specific estimates of the gradient. To cover the domain where the flamelets do not exist, non-stationary flamelets (extinguishing) flames are chosen. The lower boundary will be a mixture line, i.e., a linear trajectory that connect the unburned mixture in the state space. Figure 5 shows the initial guess constructed with this approach for a methane/air flame, using N_2 and CO_2 parametrization.

This strategy seems appropriate considering that the flamelet solution already consist in a low dimensional manifold itself. To obtain even better results, suitable boundary conditions should be applied to the flamelets, which ought to be the same as the flame to be simulated. One example could be the initial guess produced for the Sandia Flame D [1, 2], a turbulent piloted methane/air flame, presented in Fig. 6. The configuration of this flame consist in the main jet of fuel, a pilot, and a coflow of air. The initial manifold built considering the boundary conditions of the main jet, the pilot and the coflow covers a bigger region in the state space compared to the one build considering only the main jet and the coflow.

Having defined the initial guess, as the parametrization choice and the estimative of the gradients, the REDIM equation (66) is ready to be numerically solved. The next section will present an algorithm to solve it.

4.4 REDIM algorithm

The method for solving Eq. (66) proposed by Bykov and Maas [5] are based on the assumption that existence, uniqueness and smoothness of the solution. The idea is to have an algorithm that is independent on the gradient estimates and represents a better way to overcome the dependence on the spatial coordinates.

Thus, an iterative process is suggested by determining automatically the parameter gradient as a function

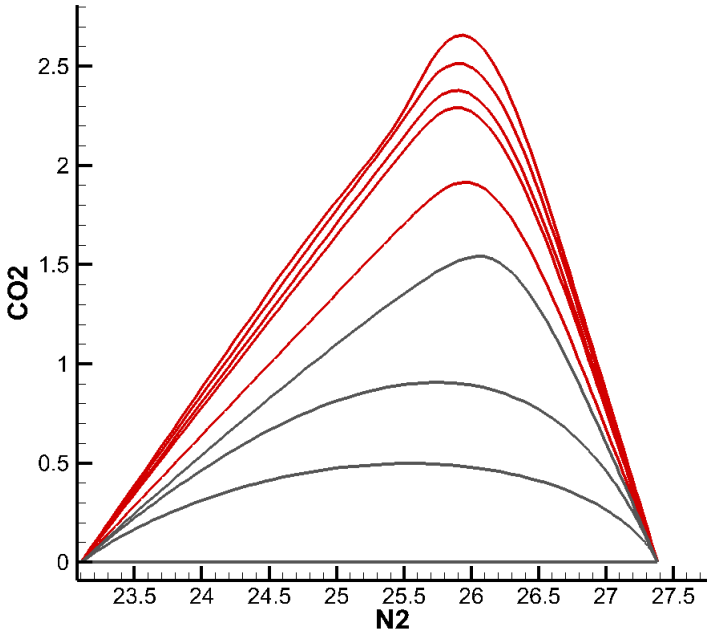

Fig. 5: Initial guess manifold for the REDIM equation based on stationary and non-stationary flamelets solutions. Red lines show stable stationary flamelets solutions, while the gray lines show extinguishing non-stationary flamelets.

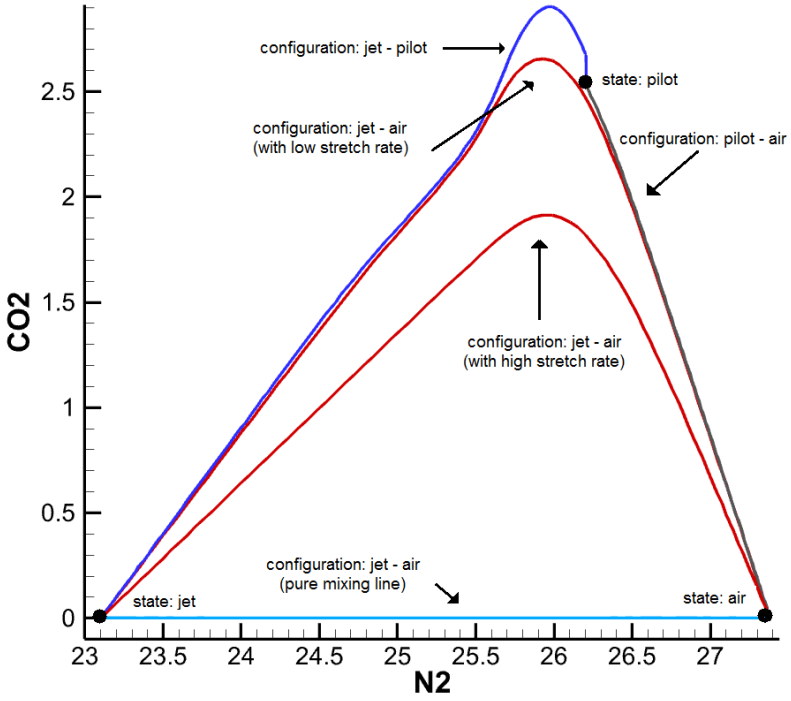

Fig. 6: Initial guess based on specific mole fractions of N_2 and CO_2 as parametrization of the REDIM. Black dots represent the different states of Sandia Flame, colored lines represent different critical flamelets of laminar counterflow non-premixed flames.

of the parameter itself. First, a constant approximation for the gradient $\mathbf{grad}(\theta) = \mathbf{c}$ is assumed for Eq. (66) in order to obtain the first approximation of the slow manifold $\mathbf{\Psi}^1(\theta)$. This constant approximation already provides an appropriate result for the reduced model, if the dimension of the reduced model is reasonably high [3].

The next step is to use the first approximation $\mathbf{\Psi}^1(\theta)$ to solve the following reduced model

$$\frac{\partial \theta}{\partial t} = \mathbf{\Psi}_\theta^{1+}\mathbf{\Phi}(\mathbf{\Psi}^1(\theta)), \tag{67}$$

which was derived from Eq. (47) using the chain rule and multiplying by $\mathbf{\Psi}_\theta^{1+}$. The solution of Eq. (67) provides a stationary solution $\theta^1(x)$ of the reduced model.

Then, θ^1 is used to correct the approximation of the gradient, making $\mathbf{grad}(\theta) = \mathbf{f}_1(\theta)$, where

$$\mathbf{f}_1(\theta) = \left.\frac{\partial \theta^1}{\partial x}\right|_{x=x^*} \tag{68}$$

The point $x = x^*$ is determined as follows: within the range of θ, a spatial coordinate x^* is defined which corresponds to some fixed value of the parameter θ^*.

With the improved approximation of the gradient, a new solution of Eq. (66) is calculated, $\mathbf{\Psi}^2(\theta)$, using $\mathbf{\Psi}^1(\theta)$ as initial guess. Then, $\mathbf{\Psi}^2(\theta)$ is used in Eq. (67) to update the gradient dependence $\mathbf{grad}(\theta) = \mathbf{f}_2(\theta)$. This iterative process is repeated until convergence is achieved.

The main steps to solve the REDIM equation an obtain the reduced slow manifold is summarized as:

1. An initial guess $\mathbf{\Psi}^0(\theta)$ is estimated for the reduced manifold;
2. The local coordinates gradient is estimated by $\mathbf{grad}(\theta) = \mathbf{f}_i(\theta)$, where $\mathbf{f}_0(\theta) = \mathbf{c}$;
3. Equation (66) is integrated to obtain a stationary solution $\mathbf{\Psi} = \mathbf{\Psi}^i(\theta)$;
4. Equation (67) is integrated to obtain a stationary solution $\theta = \theta^1$ and improve the gradients using Eq. (68);
5. Set $i = i + 1$ and return the step 2 until convergence is achieved.$\mathbf{\Psi}^2(\theta)$.

Therefore, as the gradient estimates is updated at each step of the integration, and the first estimate is always constant, the method depends only of the initial guess provided for initialization of the process.

5 REDIM calculated for ethanol

In this section, the methodology for generating the 2D-REDIM for ethanol is presented. The algorithm explained in last section was used. Therefore, it was only needed to find the initial guess for integration of Eq. (66). The variables chosen for parametrization are the specific mole fraction of N_2 and CO_2, accounting for the mixture process and the reaction progress, respectively.

The initial manifold is given by detailed simulations of counterflow non-premixed flames, varying the pressure gradient J. A non-stationary flamelet was also simulated to fill out a major part of the state space. The boundary conditions are the same as the experimental conditions used in the work of Saxena and Williams [27]. This is because the data from this work will be used to validate the REDIM. The conditions are shown in table 1. The simulations were done with the codes INSFLA and HOMREA, which integrates Eq. (66) [20].

Tab. 1: Conditions used in the simulation of counterflow flames to obtain an initial guess for REDIM. The species quantities are given in mole fractions.

	Fuel stream	Oxidizer stream
$X_{C_2H_5OH}$	0.3	0
X_{N_2}	0.7	0.79
X_{O_2}	0	0.21
Velocity (cm/s)	29.8	30
Temperature (Kelvin)	340	298
Pressure (atm)	1	1

The pressure gradient varied from $J = -1.0 \times 10^3$ to $J = -1.0 \times 10^5$, the last stable flame considered. The extinguished flame is simulated with $J = -2.0 \times 10^5$, as well as the non-stationary solutions. This is shown in Fig. 7 where the solutions are projected in the $N_2 - CO_2$ plane.

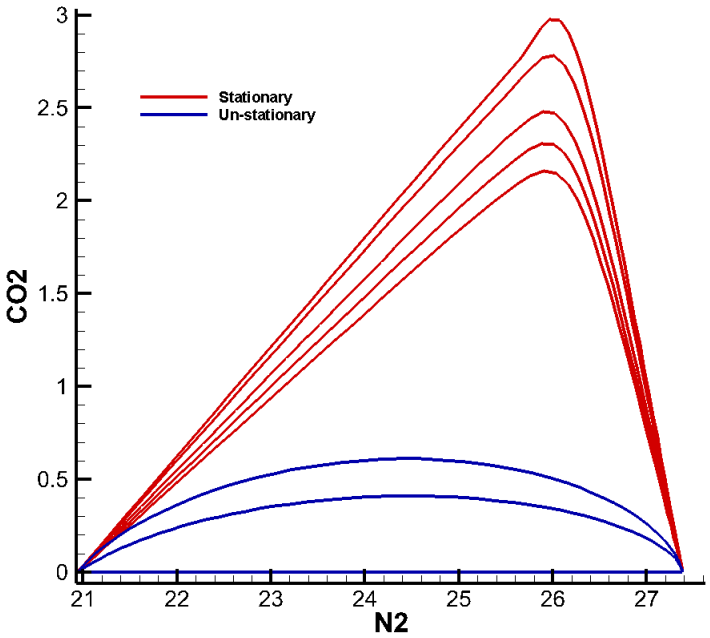

Fig. 7: Initial guess for the REDIM of ethanol based on counterflow non-premixed flames. The red lines represent the stable flames and the blue the non-stationary and extinguished flames.

The initial guess is used to start the integration of Eq. (66), where the estimation of the gradients follows the algorithm of the last section. After convergence, the REDIM built is presented in Fig. 8 in the $N_2 \times CO_2 \times OH$ and $N_2 \times CO_2$ planes. The initial counterflow flames are also displayed to show that the initial guess is already within the manifold, and thus confirming the already mentioned that the flamelet is equivalent to a 1D-REDIM. The projections of temperature, specific mole fractions of H_2O, CO and OH in the 2D-REDIM is shown in Fig. 9.

It can be observed that the reaction zone is very well defined in the REDIM in the region of high temperature. It is also in that region that important intermediate species are formed, such as CO and OH. Water is formed almost in all the region reached by the REDIM, where the highest amount is formed not in the region of the highest temperature, but slightly prior to that. This results show that the dynamics of the production/consumption of species are greatly described by the chosen parametrization.

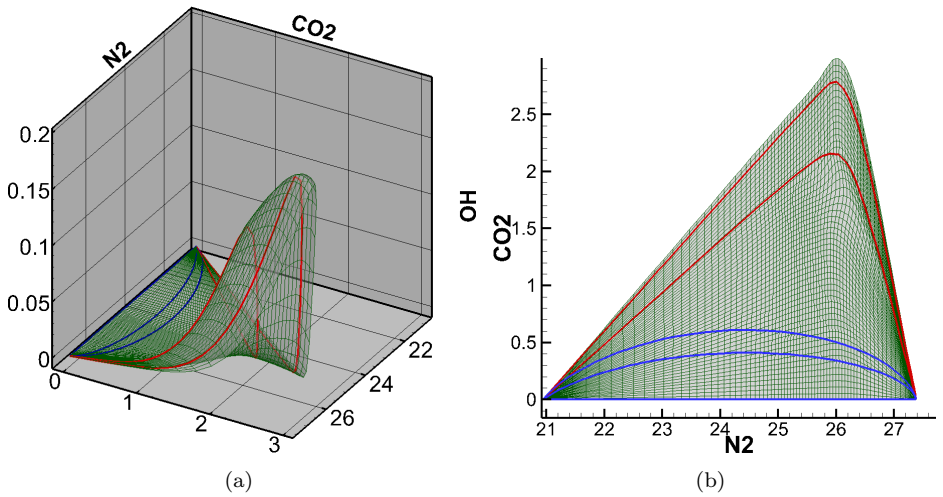

(a) (b)

Fig. 8: Representation of the REDIM in the (a) $N_2 \times CO_2 \times OH$ and (b) $N_2 \times CO_2$ planes. The initial guess is also displayed to show its validity.

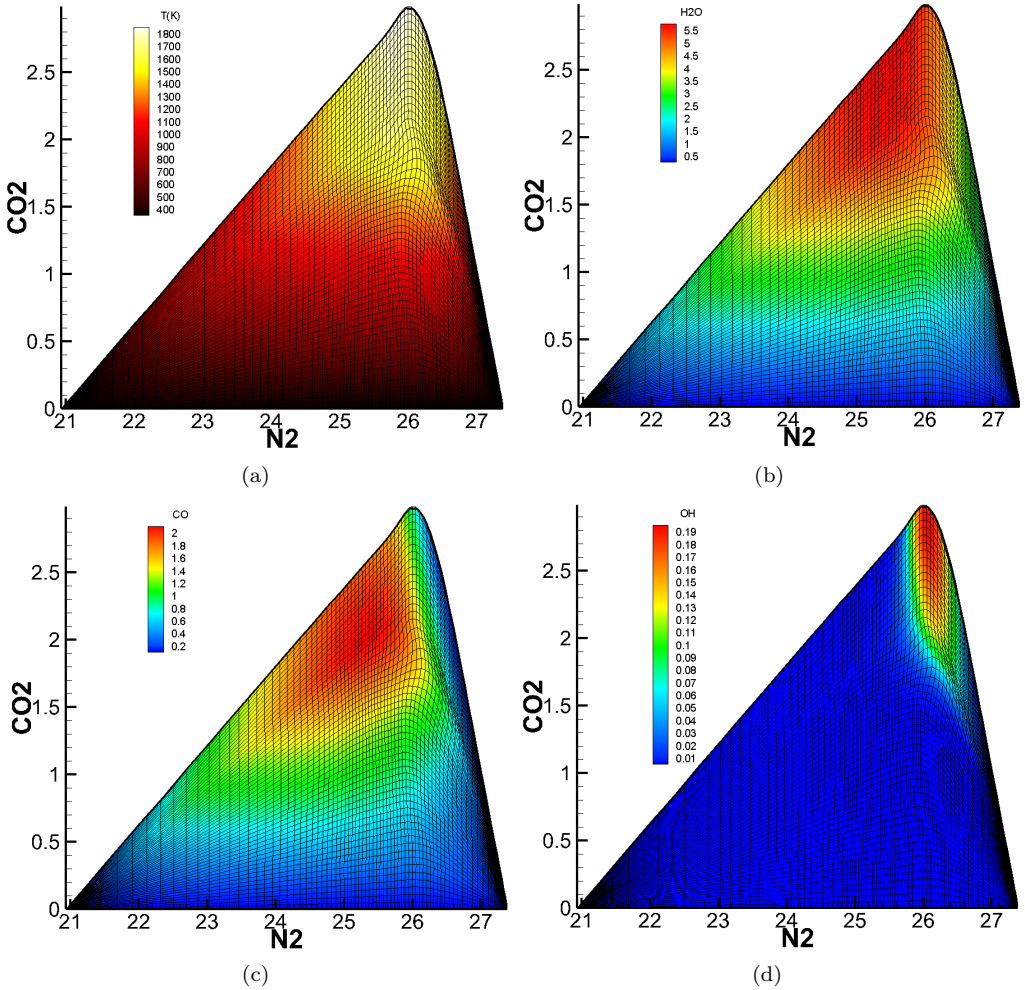

(a) (b)

(c) (d)

Fig. 9: Projections of (a) temperature and specific mole fractions of (b) H_2O, (c) CO and (d) OH in the 2D-REDIM.

References

[1] International workshop on measurement and computation of turbulent nonpremixed flames. *[Online]. Available: http://www.sandia.gov/TNF/abstract.html*.

[2] Barlow, R., and Frank, J. Effects of turbulence on species mass fractions in methane/air jet flames. In *Symposium (International) on Combustion* (1998), vol. 27, Elsevier, pp. 1087–1095.

[3] Bykov, V., and Maas, U. The extension of the ILDM concept to reaction–diffusion manifolds. *Combustion Theory and Modelling 11*, 6 (2007), 839–862.

[4] Bykov, V., and Maas, U. Extension of the ILDM method to the domain of slow chemistry. *Proceedings of the Combustion Institute 31*, 1 (2007), 465–472.

[5] Bykov, V., and Maas, U. Problem adapted reduced models based on reaction–diffusion manifolds (REDIMs). *Proceedings of the Combustion Institute 32*, 1 (2009), 561–568.

[6] Bykov, V., Neagos, A., and Maas, U. On transient behavior of non-premixed counter-flow diffusion flames within the REDIM based model reduction concept. *Proceedings of the Combustion Institute 34*, 1 (2013), 197–203.

[7] Claramunt, K., Consul, R., Carbonell, D., and Pérez-Segarra, C. Analysis of the laminar flamelet concept for non-premixed laminar flames. *Combustion and Flame 145*, 4 (2006), 845–862.

[8] Cuenot, B. The flamelet model for non-premixed combustion. In *Turbulent Combustion Modeling*. Springer, 2011, pp. 43–61.

[9] Fischer, S., Markus, D., Ghorbani, A., and Maas, U. PDF simulations of the ignition of hydrogen/air, ethylene/air and propane/air mixtures by hot transient jets. *Zeitschrift für Physikalische Chemie 231*, 10 (2017), 1773–1796.

[10] Golub, G. H., and Van Loan, C. F. *Matrix computations*, vol. 3. JHU Press, 2012.

[11] Gorban, A. N., and Karlin, I. V. Method of invariant manifold for chemical kinetics. *Chemical Engineering Science 58*, 21 (2003), 4751–4768.

[12] Goussis, D. A., and Maas, U. Model reduction for combustion chemistry. In *Turbulent Combustion Modeling*. Springer, 2011, pp. 193–220.

[13] Konzen, P. H. d. A. *Simulaçao Numérica de Chama Laminar Axisimétrica de Metano/Ar usando REDIM*. PhD thesis, Universidade Federal do Rio Grande do Sul, 2010.

[14] Konzen, P. H. d. A., Richter, T., Riedel, U., and Maas, U. Implementation of REDIM reduced chemistry to model an axisymmetric laminar diffusion methane–air flame. *Combustion Theory and Modelling 15*, 3 (2011), 299–323.

[15] Lam, S. Using CSP to understand complex chemical kinetics. *Combustion Science and Technology 89*, 5-6 (1993), 375–404.

[16] Lam, S., and Goussis, D. Understanding complex chemical kinetics with computational singular perturbation. In *Symposium (International) on Combustion* (1989), vol. 22, Elsevier, pp. 931–941.

[17] Lam, S., and Goussis, D. The CSP method for simplifying kinetics. *International Journal of Chemical Kinetics 26*, 4 (1994), 461–486.

[18] Lebedev, A., Okun, M., Chorkov, V., Tokar, P., and Strelkova, M. Systematic procedure for reduction of kinetic mechanisms of complex chemical processes and its software implementation. *Journal of Mathematical Chemistry 51*, 1 (2013), 73–107.

[19] Løvås, T., Nilsson, D., and Mauss, F. Automatic reduction procedure for chemical mechanisms applied to premixed methane/air flames. *Proceedings of the Combustion Institute 28*, 2 (2000), 1809–1815.

[20] Maas, U. *Automatische reduktion von reaktionsmechanismen zur simulation reaktiver strömungen*. PhD thesis, Institut für Technische Verbrennung, Universität Stuttgart, Germany, 1993.

[21] Maas, U., and Pope, S. Simplifying chemical kinetics: intrinsic low-dimensional manifolds in composition space. *Combustion and Flame 88*, 3 (1992), 239–264.

[22] Pepiot-Desjardins, P., and Pitsch, H. An automatic chemical lumping method for the reduction of large chemical kinetic mechanisms. *Combustion Theory and Modelling 12*, 6 (2008), 1089–1108.

[23] Peters, N. Laminar diffusion flamelet models in non-premixed turbulent combustion. *Progress in energy and combustion science 10*, 3 (1984), 319–339.

[24] Peters, N. *Turbulent combustion*. Cambridge University Press, 2000.

[25] Pitsch, H., and Peters, N. A consistent flamelet formulation for non-premixed combustion considering differential diffusion effects. *Combustion and Flame 114*, 1 (1998), 26–40.

[26] Powers, J. M. Intrinsic low-dimensional manifold method for rational simplification of chemical kinetics.

[27] Saxena, P., and Williams, F. A. Numerical and experimental studies of ethanol flames. *Proceedings of the Combustion Institute 31*, 1 (2007), 1149–1156.

[28] Schiessl, R., Bykov, V., Maas, U., Abdelsamie, A., and Thévenin, D. Implementing multi-directional molecular diffusion terms into reaction diffusion manifolds (REDIMs). *Proceedings of the Combustion Institute 36*, 1 (2017), 673–679.

[29] Steinhilber, G., and Maas, U. Reaction-diffusion manifolds for unconfined, lean premixed, piloted, turbulent methane/air systems. *Proceedings of the Combustion Institute 34*, 1 (2013), 217–224.

[30] Tomlin, A. S., Turányi, T., and Pilling, M. J. Mathematical tools for the construction, investigation and reduction of combustion mechanisms. *Comprehensive chemical kinetics 35* (1997), 293–437.

[31] Turányi, T. Reduction of large reaction mechanisms. *New Journal of Chemistry 14* (1990), 795–803.

[32] Turányi, T. Sensitivity analysis of complex kinetic systems. Tools and applications. *Journal of Mathematical Chemistry 5*, 3 (1990), 203–248.

[33] Turanyi, T., Tomlin, A., and Pilling, M. On the error of the quasi-steady-state approximation. *The Journal of Physical Chemistry 97*, 1 (1993), 163–172.

[34] Turányi, T., and Tomlin, A. S. *Analysis of kinetic reaction mechanisms*. Springer, 2014.

[35] Van Oijen, J., and De Goey, L. Modelling of premixed counterflow flames using the flamelet-generated manifold method. *Combustion Theory and Modelling 6*, 3 (2002), 463–478.

[36] Wang, P., Platova, N., Fröhlich, J., and Maas, U. Large eddy simulation of the PRECCINSTA burner. *International Journal of Heat and Mass Transfer 70* (2014), 486–495.

[37] Wang, P., Zieker, F., Schiessl, R., Platova, N., Fröhlich, J., and Maas, U. Large eddy simulations and experimental studies of turbulent premixed combustion near extinction. *Proceedings of the Combustion Institute 34*, 1 (2013), 1269–1280.